63-2-4

REPORT AN-856

296 862

FEASIBILITY DETERMINATION OF A NUCLEAR THERMIONIC SPACE POWER PLANT

CONTRACT NO. AF 33(657)-8977
PROJECT NO. 8173
TASK NO. 817305-10

QUARTERLY TECHNICAL PROGRESS REPORT
FOR PERIOD
1 NOVEMBER 1962 THROUGH 31 JANUARY 1963

Aerojet-General NUCLEONICS
A SUBSIDIARY OF AEROJET-GENERAL CORPORATION
SAN RAMON, CALIFORNIA

N O T I C E

"The work covered by this report was accomplished under Air Force Contract AF 33(657)-8977, but this report is being published and distributed prior to Air Force review. The publication of this report, therefore, does not constitute approval by the Air Force of the findings or conclusions contained herein. It is published for the exchange and stimulation of ideas."

FEASIBILITY DETERMINATION

OF A

NUCLEAR THERMIONIC SPACE POWER PLANT

Quarterly Technical Progress Report

For Period

1 November 1962 through 31 January 1963

Report AN-856

Contract No. AF 33(657)-8977
Project No. 8173
Task No. 817305-10

Reviewed by: K. E. Buck
K. E. Buck, Project Engineer

Reviewed and Approved by: K. P. Johnson
K. P. Johnson
Manager, Space Power Department

Aerojet-General NUCLEONICS
A SUBSIDIARY OF AEROJET-GENERAL CORPORATION
SAN RAMON, CALIFORNIA

TABLE OF CONTENTS

LIST OF FIGURES

LIST OF TABLES

I. OBJECTIVE

The work described in this report is aimed at demonstrating the feasibility of the Nuclear Thermionic Radiator Space Power System. It is a continuation of work initiated on Contract AF 33(616)-8119. The specific objectives of the current program are:

1) To demonstrate operation of a minimum of three thermionic converters in a series array using heat from a liquid-metal loop to heat the cathodes; and

2) To demonstrate 1000 hours of thermionic operation using liquid-metal heating.

II. INTRODUCTION

The thermionic radiator is a system which will utilize a nuclear heat source to produce electrical power in space. A combined thermionic converter-radiator unit is coupled with a high temperature, liquid metal cooled, fast reactor heat source; coolant is circulated directly through the radiator and back to the reactor in a single loop. A cylindrical thermionic converter filled with cesium vapor encircles the tube walls of the radiator. The emitter (on the radiator tubes) is heated by conduction through the tube wall. Collectors are concentric to the cahtode and dissipate waste heat directly to space through attached fins.

A brief description of the considerations instrumental in selection of the type of thermionic converter and liquid metal loop to be used was given in the report for the previous quarter (AN-778). The converters are of a type being developed by RCA under Contract AF 33(657)-8005. The converters are cylindrical and will be mounted on a columbium alloy tube, using an electrically insulating thermal bond. The liquid-metal loop, on which these converters will be mounted, will be fabricated from the same columbium alloy. Lithium will be circulated in the loop by natural convection. The entire system will be placed in a vacuum chamber to protect the refractory metals from oxidation.

In addition to the above experimental work, a thermal transport analysis is being conducted to aid in selection of loop test parameters and to study over-all system characteristics.

Status at the present time is as follows:

1) The thermal bond investigation being conducted at AGN is complete.

2) The thermal transport analysis is in progress; some results are presented in this report.

3) Design of the test loop is essentially complete. Fabrication will be completed during the next quarter.

III. TECHNICAL PROGRESS

Technical work on this program has been divided into the following three tasks:

Task 2 - Liquid Metal Tubing - Converter Bond

Task 3 - Thermal Transport Analysis

Task 4 - Series Unit Loop Test

Technical progress on each task is discussed below.

A. TASK 2 - LIQUID METAL TUBING - CONVERTER BOND

A major portion of this task was completed during the previous quarter and is reported in AN-778. Four additional bonds have been made and evaluated, completing this task. The results are summarized below.

1. General Approach

Bonds investigated under this program are based on the use of plasma-sprayed alumina as an electrical-insulating thermal-conducting material. In all cases, the alumina is plasma-sprayed onto columbium tubing, and molybdenum is then plasma-sprayed over the alumina. The bond is then completed by brazing an outer molybdenum sleeve to the metallic coating on the alumina.

2. Alumina Coatings

No plasma-spraying was done during this quarter, but results of the brazing tests affected some of the previous conclusions concerning the alumina coating. The four recently completed bonds were made with unsintered alumina coatings, and in every case there was some separation between the alumina and the columbium. In the bond made during the previous quarter, only sintered alumina was used and no separation was observed. These results indicate that sintering results in a definitely improved adhesion between the columbium and alumina. This is contrary to previous results in which little, if any, improvement due to sintering was observed.

3. Brazing Studies

Bonds fabricated during this quarter used the brazing techniques listed below.

Braze Material	Brazing Temperature	Time at Temperature
Nickel	2725°F	10 minutes
Ni-35Mo-5Fe	2650°F	10 minutes
Titanium	3080°F	10 minutes
Titanium	3030°F	2 minutes

Excellent results were obtained with the nickel and the Ni-Mo-Fe brazing alloys. These brazes resulted in good filling and good bonds across the joint (Mo-Braze-Mo powder-alumina), but a 1 to 2 mil gap was observed between the Cb tube and the plasma-sprayed alumina (Figures 1 through 4).

The Ni and the Ni-Mo-Fe brazing alloys completely alloyed with the plasma-sprayed molybdenum powder, and considerable densification of this layer has occurred, as shown by Figures 1 through 4. Some evidence of diffusion of the brazing alloy into the molybdenum outer cylinder, for a depth of about 3 mils, is seen in Figure 4.

The first braze, using pure Ti as the filler, utilized a sample which had a 0.5 to 1 mil plasma-sprayed coating of Mo in the alumina; the brazing temperature was 3080°F, and the time at temperature was 10 minutes. This sample was electrically shorted after the brazing operation; subsequent metallographic analysis showed that the Ti had reacted with the thin Mo powder coating and with the alumina powder coating, filling the pores, diffusing through them, and shorting out to the Cb tube where it filled a 2 mil gap between the Cb tubing and the alumina (Figures 5 and 6).

The reactivity of titanium with aluminum is well known, and this can be an advantage or disadvantage, depending on the parameters involved in the test; if these are known and controlled, good braze joints

FIGURE 1. Ni BRAZE

200X
POLISHED

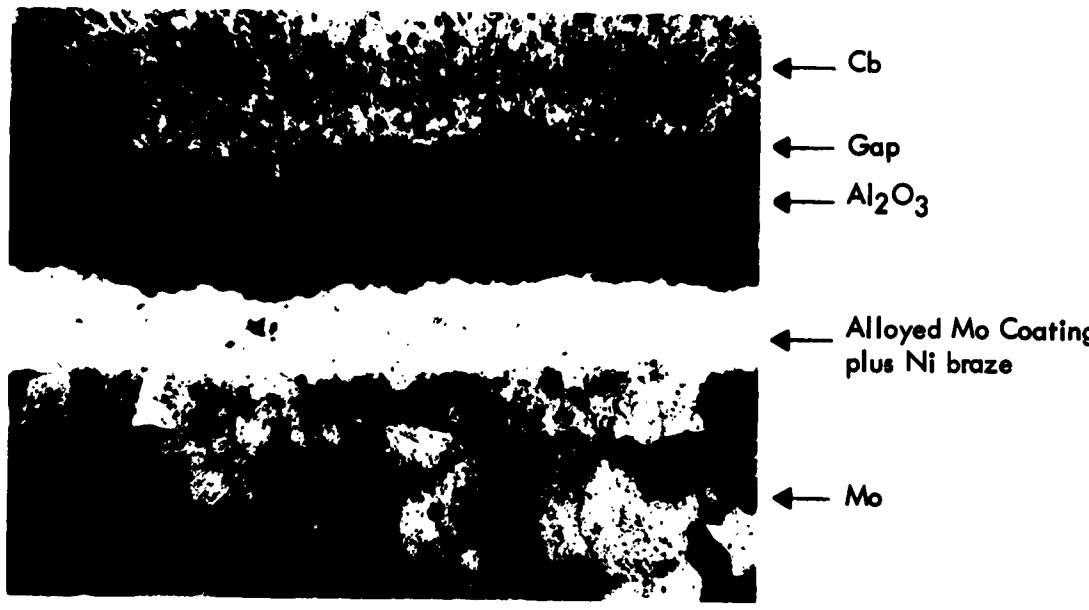

FIGURE 2. Ni BRAZE

100X
ETCHED

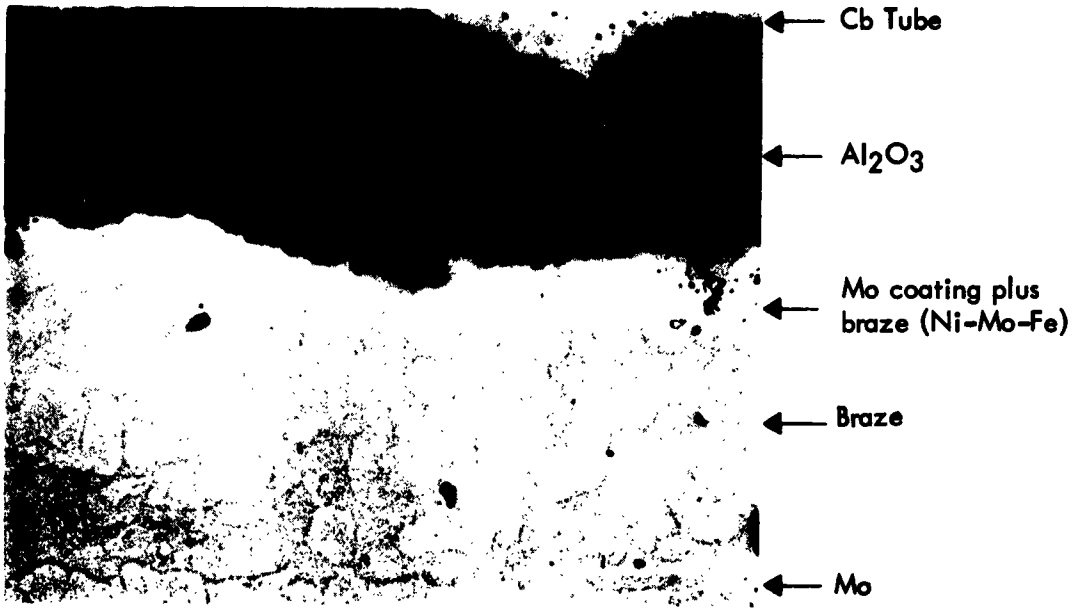

FIGURE 3. Ni-Mo-Fe BRAZE

200X
POLISHED

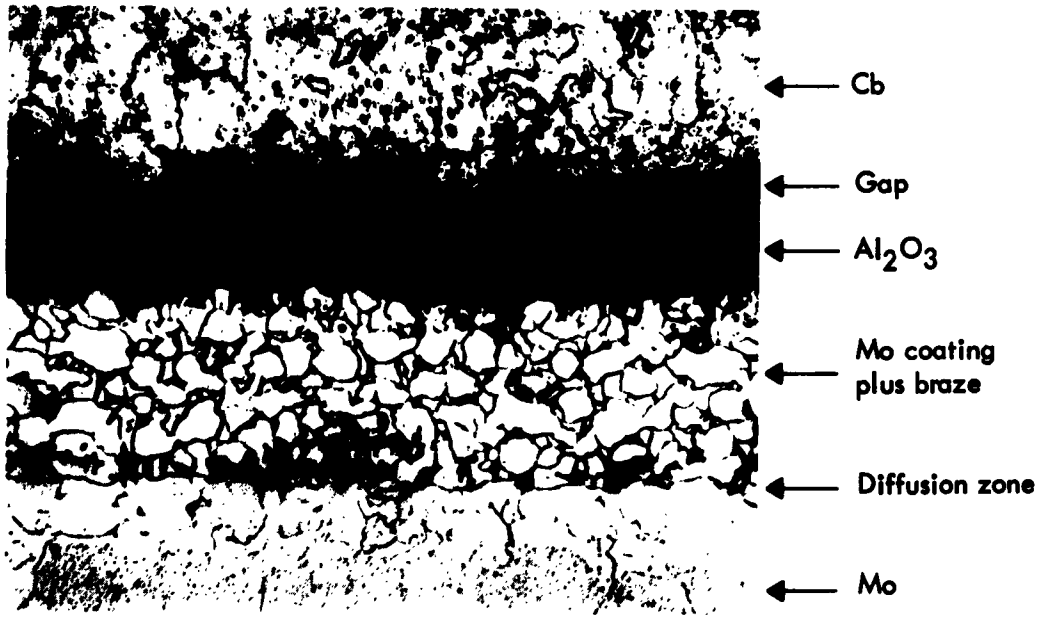

FIGURE 4. Ni-Mo-Fe BRAZE

100X
ETCHED

170-63-751

Cb Tube

Diffused alloy (Ti+Mo) which filled gap

Al_2O_3 with Mo-Ti inclusions

Mo-Ti

Mo

200X
POLISHED

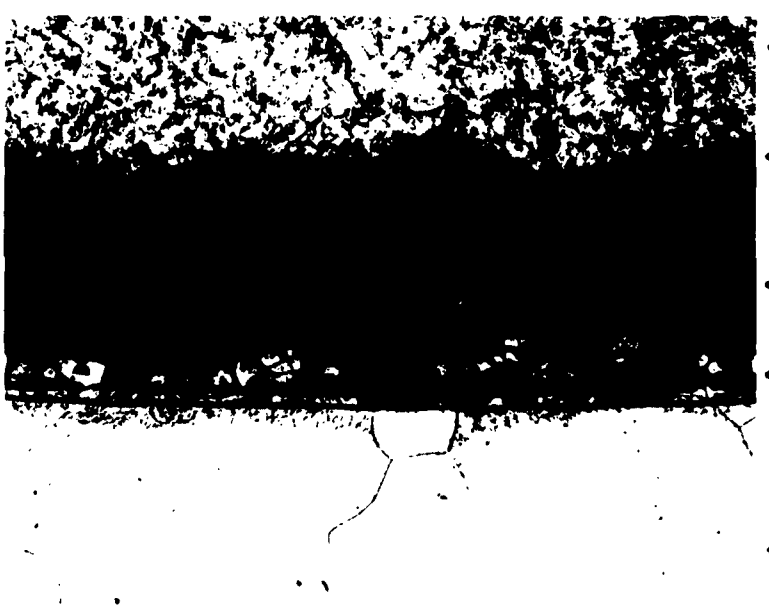

Cb

Gap left by the etching out of the Ti-Mo+

Al_2O_3 (Ti-Mo inclusions etched out)

Braze (Ti-Mo+ etched out)

Mo

100X
ETCHED

17.0-63-752

between Al_2O_3 + Mo sprayed Cb tubes and Mo concentric tubes can be obtained. The parameters which influenced the results were:

1) Temperature

2) Time at temperature

3) Conditions and thickness of the Mo barrier coating (sprayed powder of high surface area)

4) Conditions of alumina coating (surface area, porosity, type of porosity)

All these conditions were favorable for a Ti-Al_2O_3 reaction; especially the time at temperature, the porosity of the alumina (15 to 20% with mostly connecting pores), and the Mo coating thickness (0.5 to 1 mil).

The titanium braze run was repeated, using a sample which had a Mo coating 5 to 6 mils thick. The brazing temperature was 3030°F and it was held only 2 minutes; the results are shown in Figures 7 and 8. No apparent excessive reaction occurred between the Ti and the Mo powder, nor any diffusion of the Ti through the Mo or the Al_2O_3. The sample was not electrically shorted, and good filling of the braze joint was achieved. The 1 to 2 mil gap between the Al_2O_3 and the Cb tube, noticed in all of the unsintered samples, is also evident in this sample.

4. Conclusions

Ni, Ni-Mo-Fe, and Ti alloys are suitable for use as brazing alloys in the thermionic power converter bond. Further screening should be conducted on the basis of diffusion rates of these alloys into the Mo and alumina at the converter operating temperature (2200°F).

An improvement in the adhesion of the Al_2O_3 coating to the Cb tubes is necessary for good thermal conductivity. This could be achieved by either improving plasma spray techniques, or by sintering the alumina coatings prior to brazing. The second method may be preferred, since it also increases the density of the alumina, hence further improving the thermal and insulating properties of the bond.

FIGURE 7. Ti BRAZE (3030°F, 2 MIN) 200X POLISHED

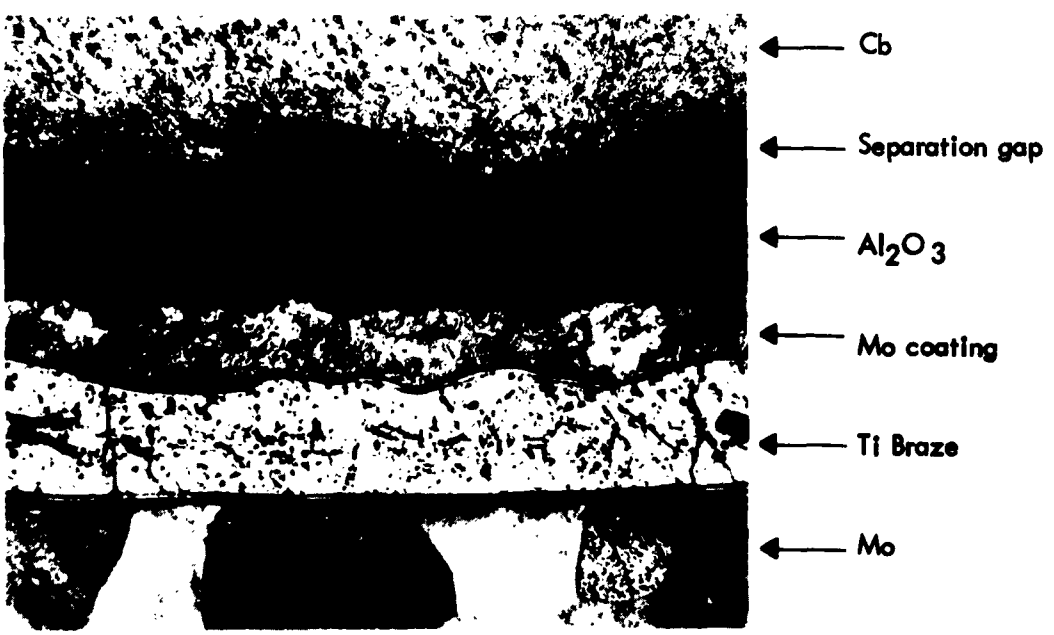

FIGURE 8. Ti BRAZE (3030°F, 2 MIN) 100X ETCHED

B. TASK 3 - THERMAL TRANSPORT ANALYSIS

A detailed outline of the work to be accomplished under this task was included in the previous quarterly report, AN-778. The effort during this quarter has been directed to heat rejection problems and the characteristics of the reactor to be used in the thermionic radiator system. The results of this work are described below.

1. Heat Rejection

Thermal radiation is the only means available for dissipating waste heat from any thermodynamic process in space. For an ideal Carnot cycle, minimum radiator area occurs when the absolute temperature of the radiator is three-fourths that of the maximum cycle temperature. The characteristics of a particular power conversion process will generally alter the temperature at which minimum radiator area occurs.

Operating a thermionic converter with a collector temperature three-fourths that of the emitter temperature is beyond current technology of low temperature thermionic conversion. At present, maximum power density in a cesiated, refractory metal converter is achieved with a collector temperature of about six-tenths of the emitter temperature. It is reasonable to expect that with a moderate development effort, higher rejection temperatures can be achieved with only a small decrease in converter power density. However, since experimental data is lacking, heat rejection calculations were made for a range of anode temperatures, converter power densities, and efficiencies.

a. Fin Calculations

Optimized linearly tapered planar fins were found for the range of radiator operating conditions shown below:

Anode outer diameter, inches - 0.8, 1.0, 1.2, 1.4
Anode surface temperature, ^{o}F - 1250, 1350, 1450, 1550, 1650
Electrical power density, w/cm^2 - 1, 2, 3
Converter efficiency, % - 8, 10, 12

Curves are given from which optimum fin dimensions and weights may be found for the range of variables indicated above.

Figure 9 is a schematic diagram of the converter configuration analyzed in this study. The finned anode rejects energy to space. Symmetrical trapezoidal planar fins were selected as the best compromise among cooling efficiency, weight, strength, and fabricability.

The parameters which affect the fin requirements are heat rejection rate, root temperature, incident flux, surface emittance, materials, and geometry. Since the heat fluxes, temperatures, and anode diameters were established as parameters during this study, the resulting radiant heat transfer analysis can be made independent of converter characteristics and design. Assumptions must be made, however, for view factors, surface characteristics, incident fluxes, and materials.

Preliminary investigations indicated that beryllium is the most suitable fin material because of its relatively low density and high thermal conductivity. Beryllium will require some bond development work, and mechanical problems may result from the difference in thermal expansion coefficients between beryllium and the refractory metal anode. Pyrolytic graphite is another candidate fin material, but its use poses structural difficulties.

Due to the geometry of space radiators, there is radiant interchange between the fins, tubes, vehicle, and space. Thermal energy impinges on the radiator from space and some is absorbed and has to be re-emitted. This incident thermal radiation consists of 1) direct solar irradiation, 2) radiation from a planet caused by its temperature, and 3) solar radiation scattered by a planet back into space. The maximum heat fluxes encountered in a 300 nautical mile orbit around Venus, Earth, and Mars are 1460 Btu/hr-ft^2, 640 Btu/hr-ft^2, and 250 Btu/hr-ft^2, respectively. Since the heat fluxes associated with the anode temperatures are significantly higher than those absorbed from space, the incident solar flux is neglected.

Substantial effort is now being expended to obtain a stable, high temperature, emissive coating. From results to date, 0.85 seems a reasonable coating emissivity. This value will be used in this analysis.

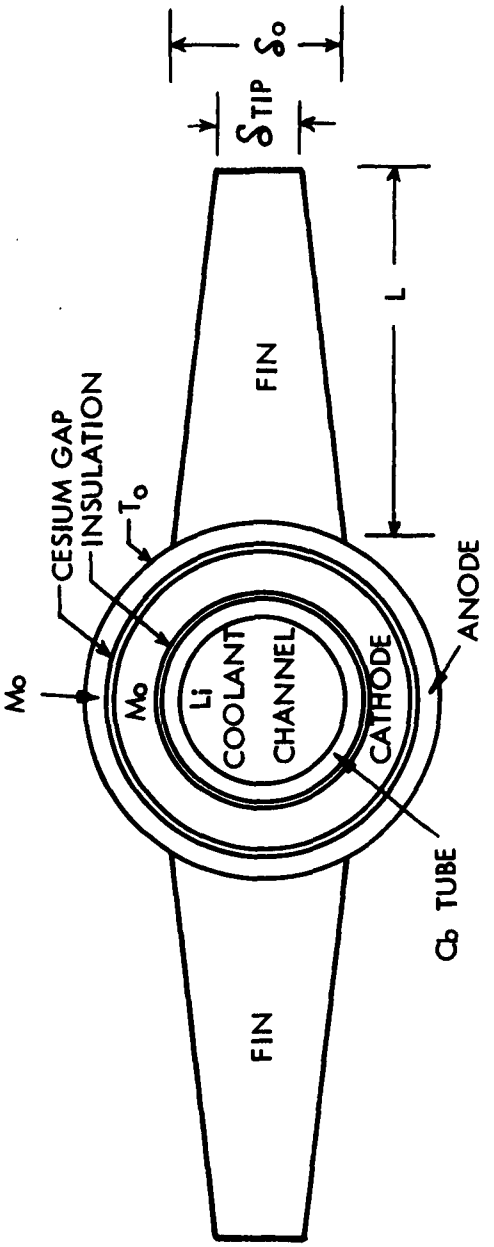

FIGURE 9. TYPICAL CONVERTER CONFIGURATION

The fin configuration in thermionic radiators affects electrical lead design, micrometeorid shielding requirements, and manifold design, all of which are very pertinent to fin optimization. For example, when structural weights are considered, optimum fins tend to be stubbier. However, since this is a preliminary study and radiator configurations have not been established, perturbations of this sort cannot be considered.

The most direct optimization procedure for linearly tapered fins is that presented by Reynolds.* Reynolds solves the generalized differential equation with the aid of a digital computer, and plots the results as a function of dimensionless parametric relationships from which optimum fins can be derived. These techniques will be employed throughout this study.

Using Reynolds' nomenclature, the assumptions and basic parameters employed in the analysis can be expressed as follows:

S = Absorbed incident solar heat flux = 0

ϵ = Surface emissivity = 0.85

W'' = Structural weight/fin area = 0

δ_{tip} = Tip thickness = 0.050 in.

$\bar{F}_{fin}$ = View factor, fin-to-space = 0.95

$\bar{F}_{tube}$ = View factor, tube-to-space = 0.85

K_{fin} = Thermal conductivity of fin = 53 Btu/hr-ft-$^{\circ}$F

The tip thickness and view factors are based on estimates of manufacturing limitations and upon similar calculations performed for the SNAP-8 radiator. The required parameters become:

---

* W. C. Reynolds, "A Design-Oriented Optimization of Simple Tapered Radiating Fins", ASME 62-WA-192.

$$A = \frac{S}{N\sigma\epsilon F_f T_o^4} = 0$$

$$H = \frac{W''}{\gamma\delta_{min}} = 0$$

$$\delta_{min} = \frac{(q')^2}{2KT_o N\sigma\epsilon\bar{F}_f T_o^4 \,(1/5 - A + 4/5\, A^{5/4})} = \frac{5(g')^2}{4K\sigma\epsilon\bar{F}_f T_o^5}$$

$$= \frac{5(q')^2 \times 12}{4 \times 53 \times 0.1714 \times 0.85 \times 0.95 \left(\frac{T_o}{100}\right)^4 T_o}$$

$$= 2.04 \frac{(q')^2}{\left(\frac{T_o}{100}\right)^4 T_o}, \text{ where } \delta_{min} \text{ is in inches}$$

$$L_{min} = \frac{q'}{N\sigma\epsilon F T_o^4 - S} = \frac{q'}{2\sigma\epsilon F T_o^4} = \frac{q' \times 12}{2 \times 0.1714 \times 0.85 \times 0.95 \left(\frac{T_o}{100}\right)^4}$$

$$= 43.3 \frac{q'}{\left(\frac{T_o}{100}\right)^4}, \text{ where } L_{min} \text{ is in inches}$$

q' = heat transfer rate per unit span per fin = Btu/hr-ft

A cursory look at the specified parameters indicated the following range for q' rejected by one fin.

q' (one fin) = 2000 Btu/hr-ft to 20,000 Btu/hr-ft

To circumvent a trial and error solution, fin configurations which will reject the q' specified above have been determined as a function of the specified root temperatures. The results of these calculations are

shown in Figures 10 and 11. Figure 11 is a replot of the data in Figure 10 for the lower ranges. The relationship between these curves and the specified parameters will now be established. The assumption is made that the anode temperature is constant and equal to the fin root temperature. The section following this one demonstrates that this assumption may be invalid, so circumferential variation in anode temperature must be considered in the final analysis. This perturbation depends on micrometeorite armor requirements (anode thickness) and upon other parameters which have not yet been thoroughly investigated.

After the fin configurations have been determined, the tube heat rejection rates can be derived from the following equation for the specified range of anode diameters and temperatures:

q'_{tube} = heat rejected by tube per unit span

$$= \sigma \epsilon \bar{F}_t T_o^4 \left[\pi D_o - 2 \delta_o \right]$$

$$= 0.1714 \times 0.85 \times 0.85 \left(\frac{T_o}{100} \right)^4 \left[\frac{\pi}{2} D_o - \delta_o \right] \frac{2}{12}$$

$$= 0.0206 \left(\frac{T_o}{100} \right)^4 \left[1.57 D_o - \delta_o \right] \text{ where } D_o \text{ and } \delta_o \text{ are in inches.}$$

The total converter heat rejection rate per unit span is given by

$$q'_{total} = 2q'_{one\ fin} + q'_{tube}$$

For the specified range of variables, then, the total converter heat flux is:

$$q''_{total} = \left(\frac{12}{\pi D_o} \right) q'_{total} = \frac{12}{\pi D_o} \left[2q'_{one\ fin} + q'_{tube} \right]$$

Hence, the relationship between Figures 10 and 11 and the initial parameters has been established. A restriction in the analysis is that $\delta_o \leq D_o$, or

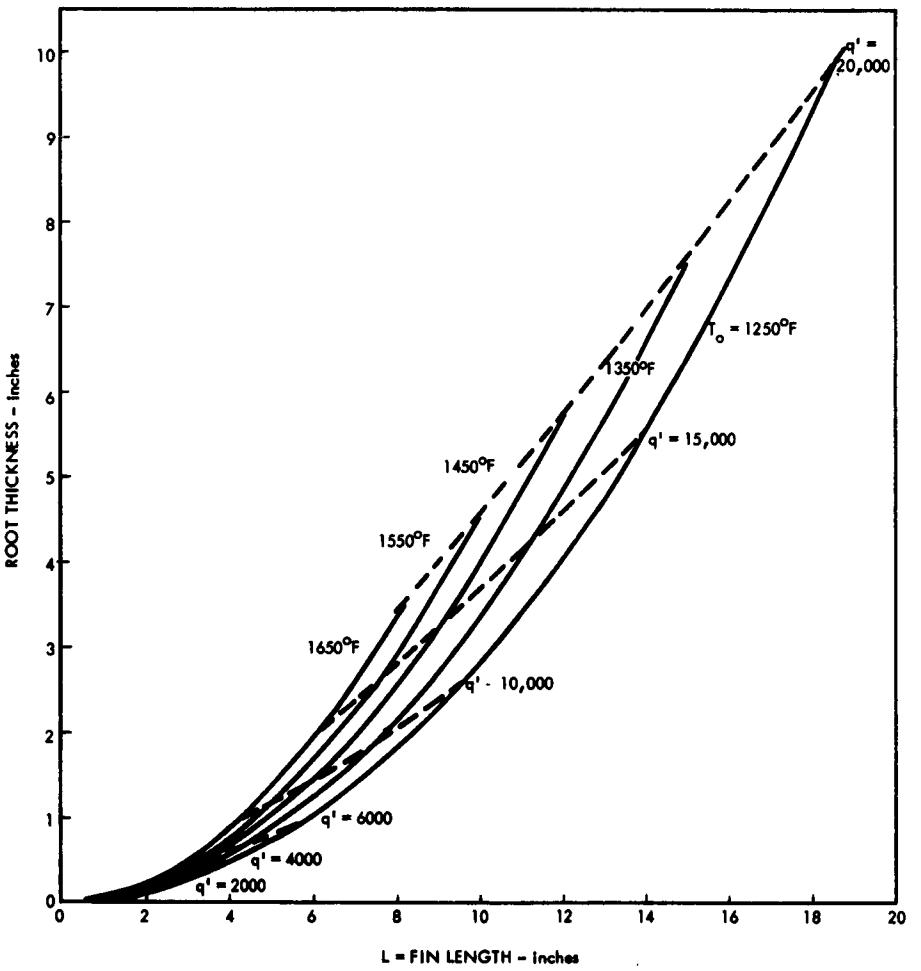

FIGURE 10. OPTIMIZED FIN CONFIGURATIONS FOR VARIOUS q' AND T_o

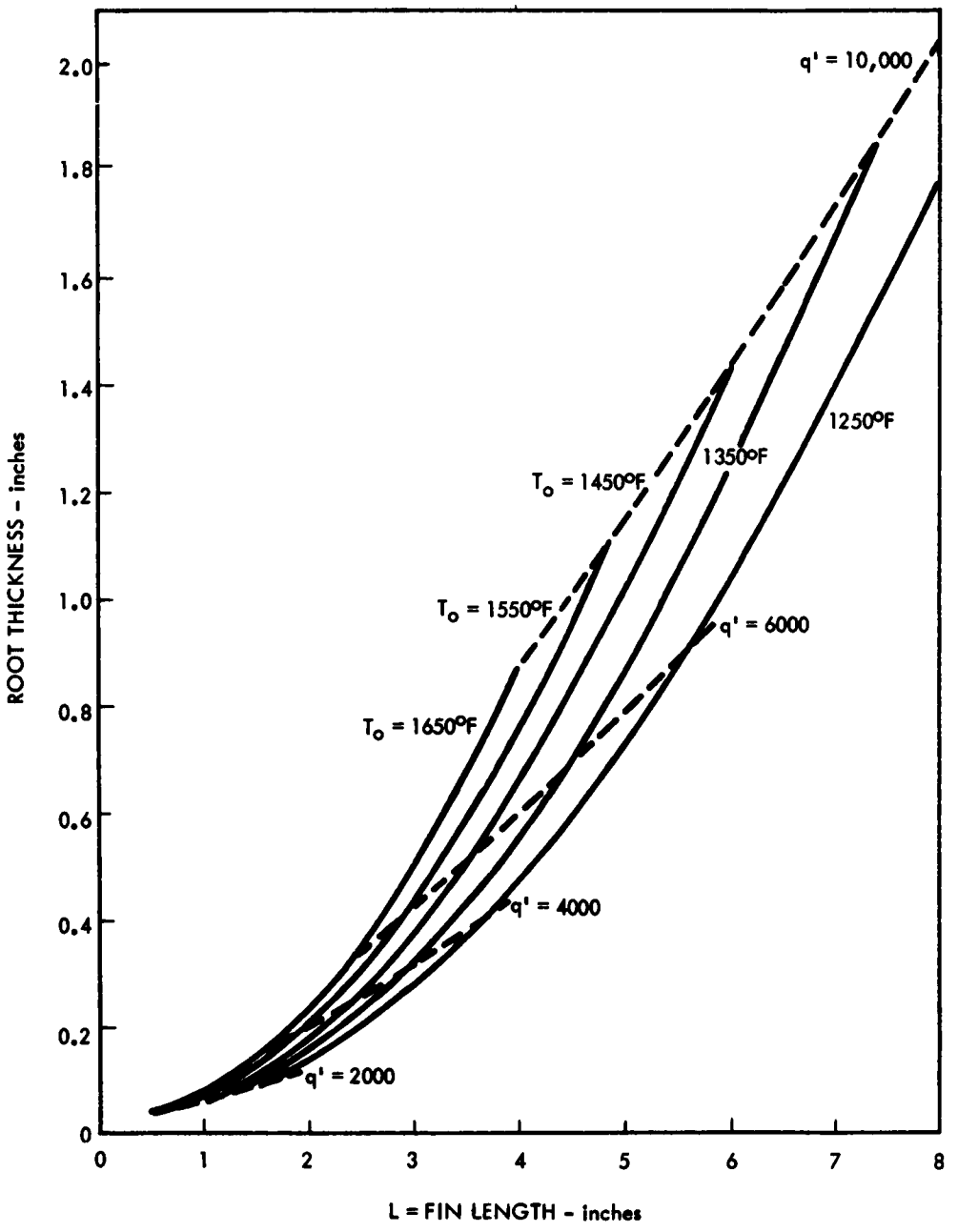

FIGURE 11. OPTIMIZED FIN CONFIGURATIONS FOR VARIOUS q' AND T_o, LOWER RANGES

the fin root thickness, should not exceed the anode diameter. Figures 12 through 15 are plots of anode power density, q" total versus q' (one fin), at a fixed D_o, over the specified anode temperature range.

The procedure for using these data is as follows. The anode power density (q''_{total}) at the outer surface of the radiator tube is calculated from: the electrical power density at the emitter, the over-all efficiency, and the ratio of the outer tube area and the emitter area. The fin heat rate (q'_{fin}) can be determined from Figures 12 through 15 if the appropriate radiator tube diameter (D_o) and fin base temperature (T_o) are used. Having established fin heat rate, the fin dimensions and weight can be found from Figures 10, 11, and 16.

A sample calculation is shown for the following conditions:

$q''_{thermal}$ = 15 w/cm^2 = 47,700 Btu/hr-ft^2
(equivalent to an output power density of 2 w/cm^2, an efficiency of 10% and an area ratio of 1.2:1)

T_o = 1400^{o}F

D_o = 1 inch

From Figure 14

q''_{fin} = 4700 Btu/hr-ft

From Figure 12

Fin root thickness = 0.38 in.

Fin length = 3.1 in.

and from Figure 16

Fin weight = 0.085 lb/in.

Circumferential temperature variation in the collector for conditions similar to those used above is calculated at the end of the next section.

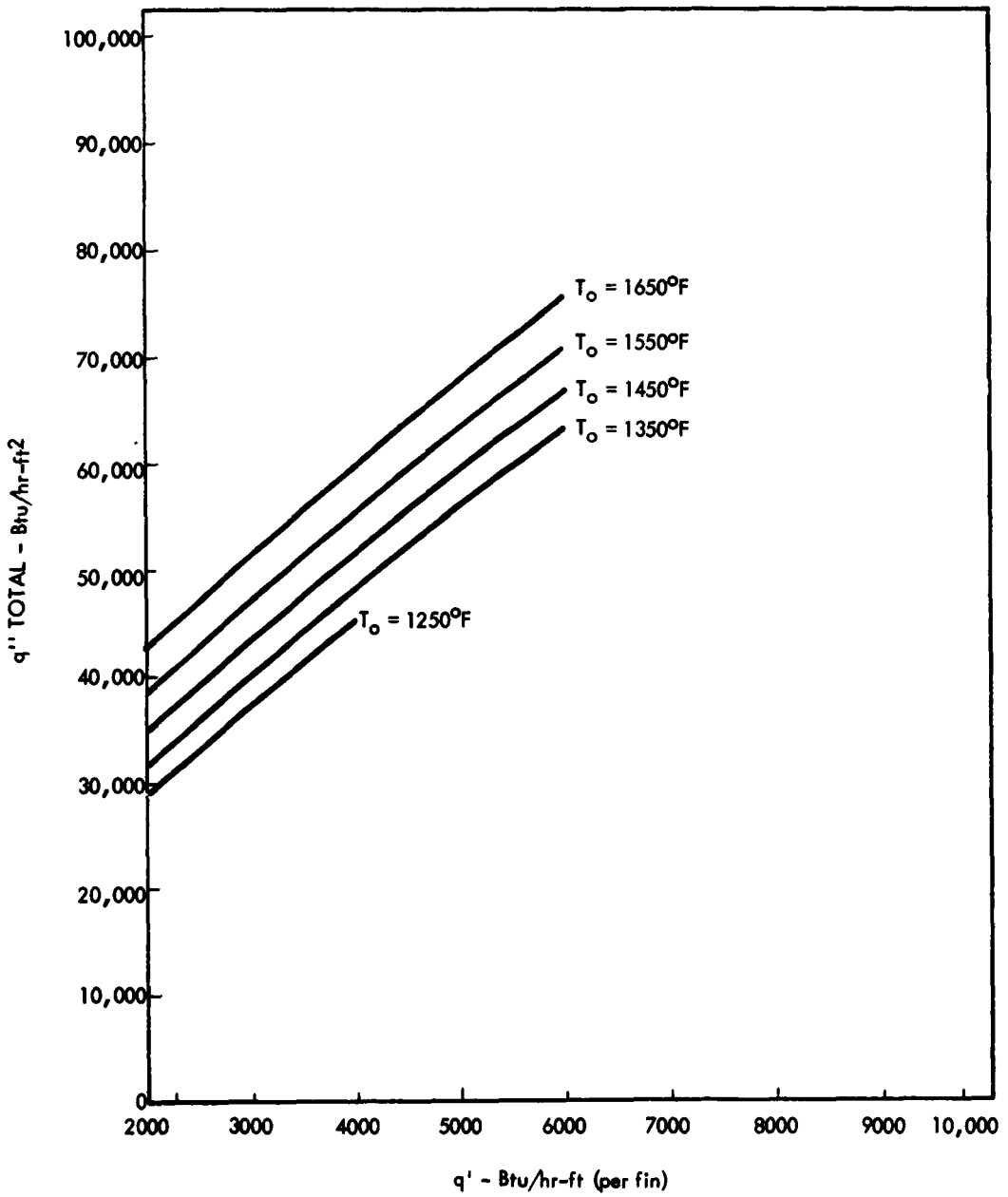

FIGURE 12. ANODE POWER DENSITY VERSUS q' FOR VARIOUS T_o WITH D_o = 0.8 inch

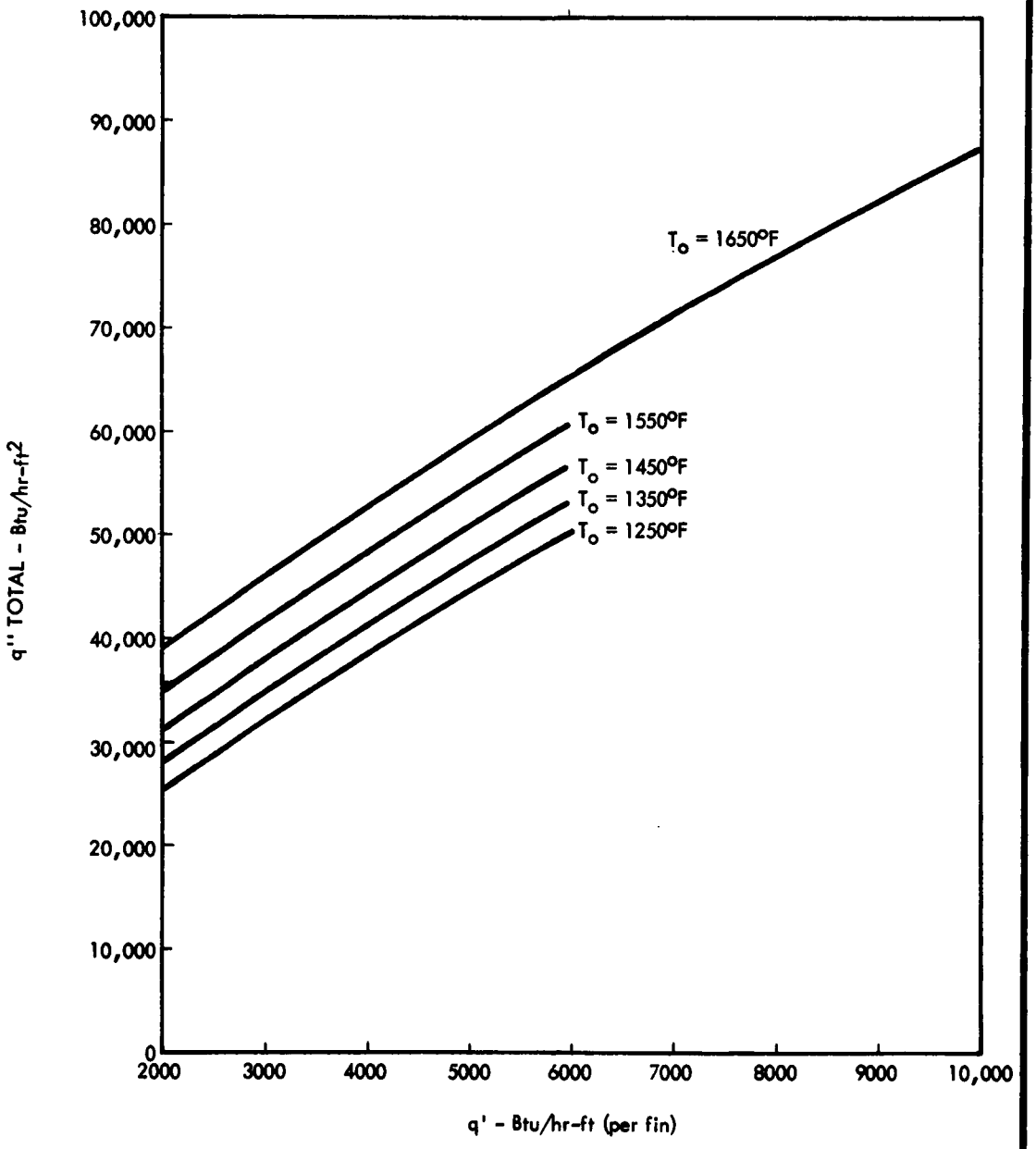

FIGURE 13. ANODE POWER DENSITY VERSUS q' FIN FOR VARIOUS T_o WITH D_o = 1.0 Inch

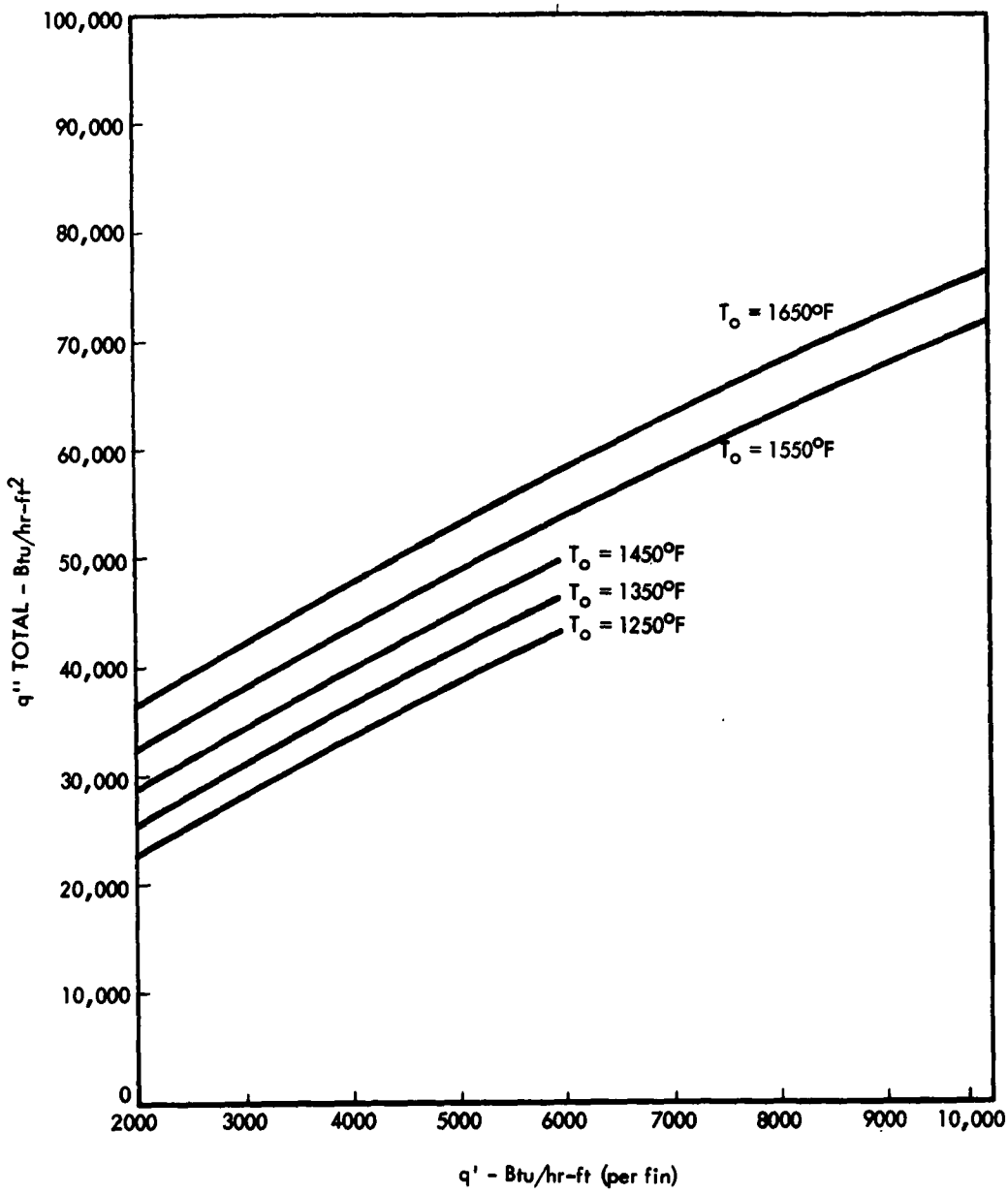

FIGURE 14. ANODE POWER DENSITY VERSUS q' FIN FOR VARIOUS T_o WITH D_o = 1.2 inches

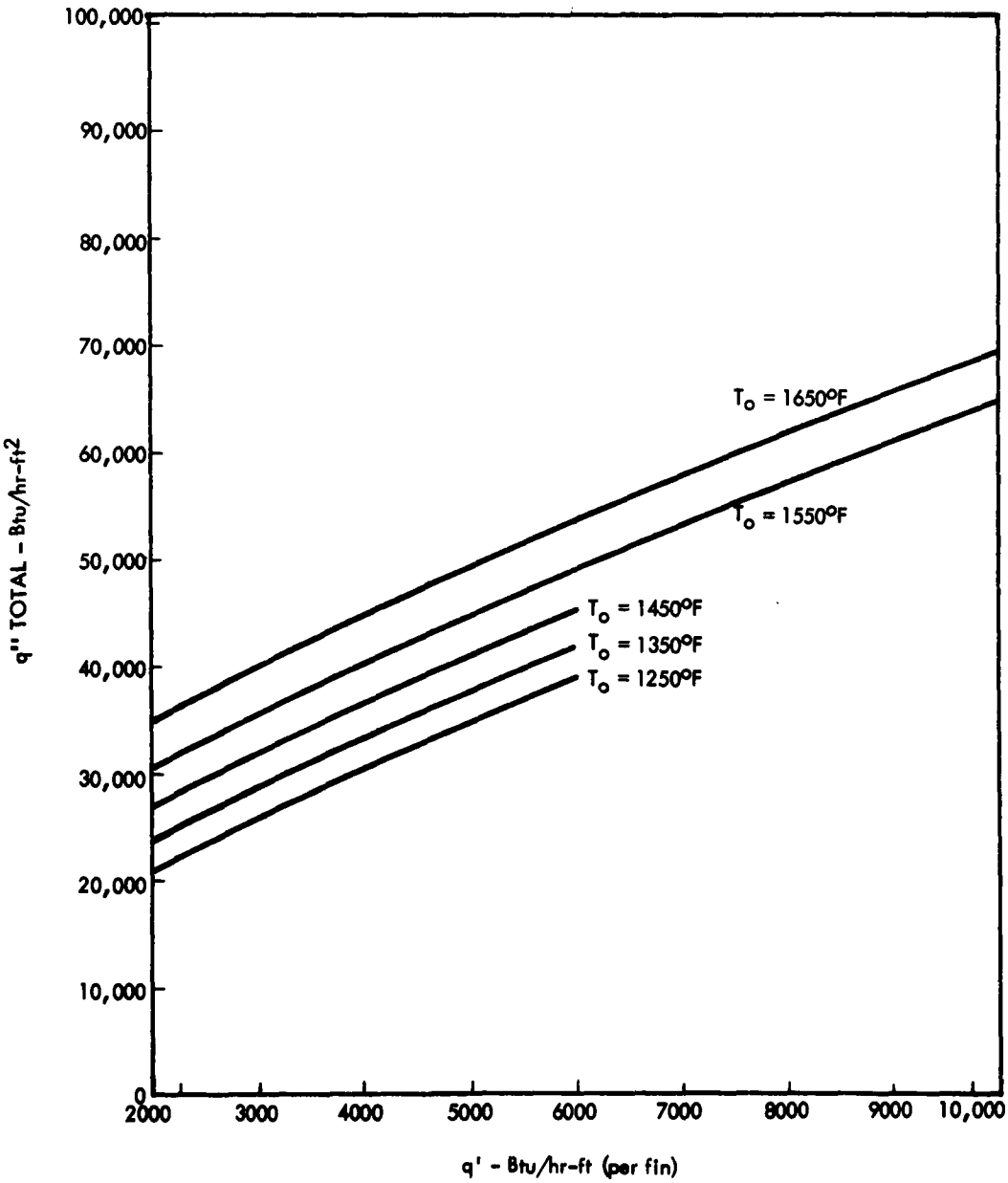

FIGURE 15. ANODE POWER DENSITY VERSUS q' FIN FOR VARIOUS T_o WITH D_o = 1.4 inches

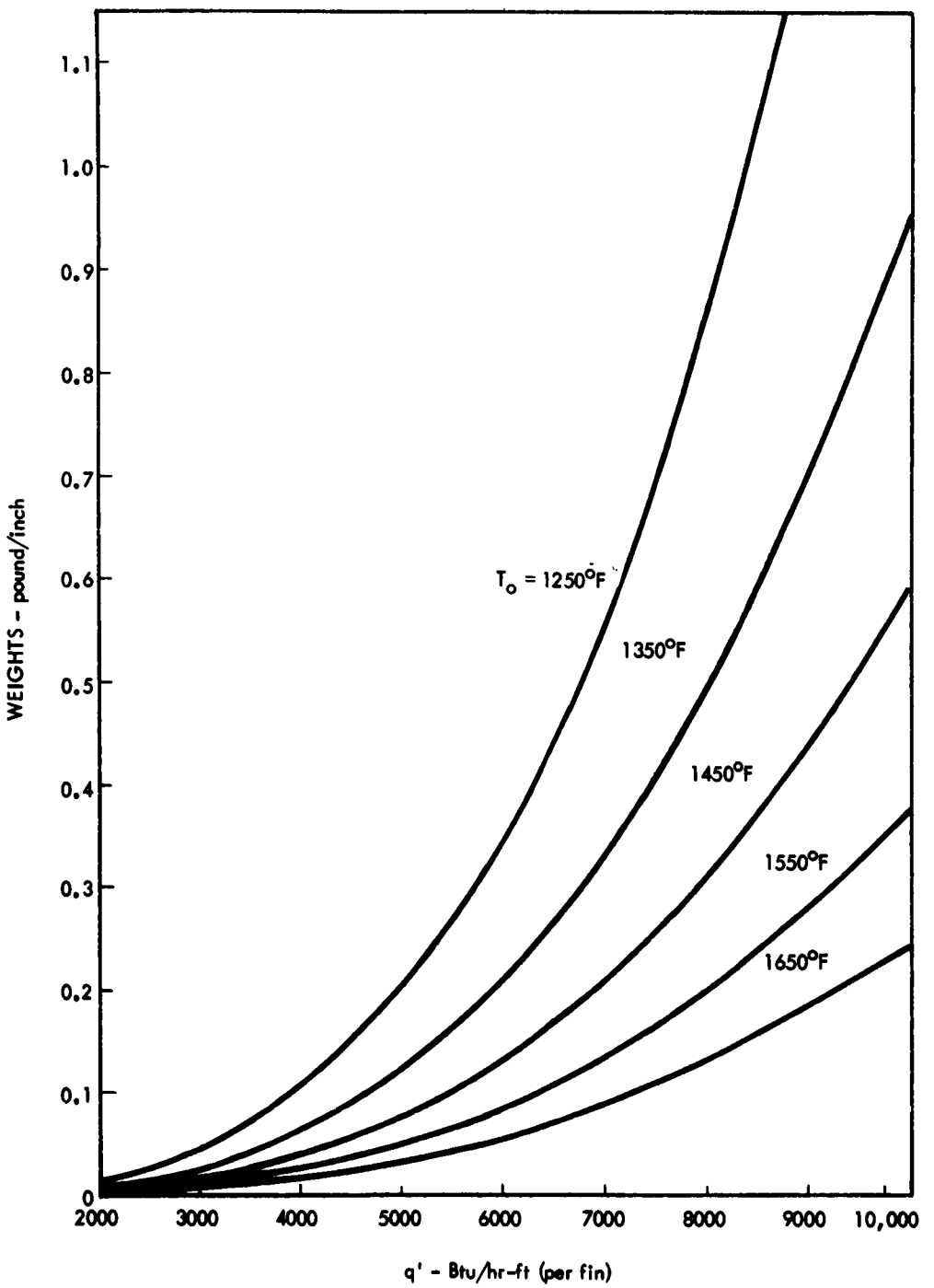

FIGURE 16. FIN WEIGHT PER UNIT LENGTH VERSUS q' FIN FOR VARIOUS T_o

b. Circumferential Temperature Variation in Collector

The high heat fluxes at which thermionic radiators operate can create substantial circumferential temperature variations in a thin anode when planar fins are attached. Since converter performance is sensitive to anode temperature, a large variation is undesirable. The following generalized analysis was made to determine the magnitude of this temperature variation as a function of geometry, anode temperature, material, and heat flux. Curves in Figures 17 and 18 give the temperature distribution and gradient as a function of basic parametric relationships. The idealizations employed in the analysis were:

1) One dimensional conduction, $T = T(x)$
2) Uniform heat flux across the electrode gap, q''_d = constant
3) External radiation heat flux given by $q'' = \sigma\epsilon_F T^4$
4) Uniform anode thickness

From symmetry arguments, the analysis may be limited to a quarter circumference of the converter as shown in the following diagram:

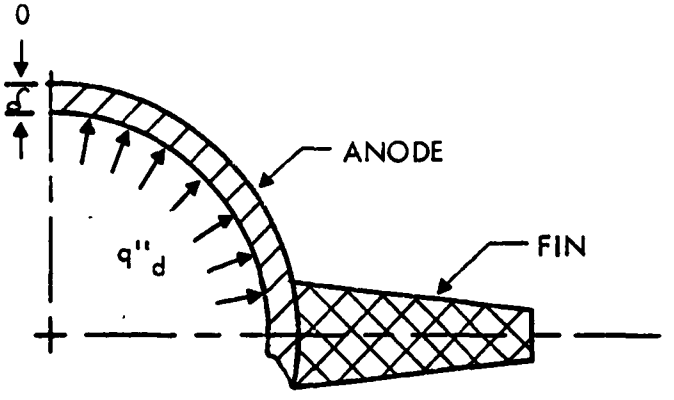

FIGURE 17. TEMPERATURE DISTRIBUTIONS

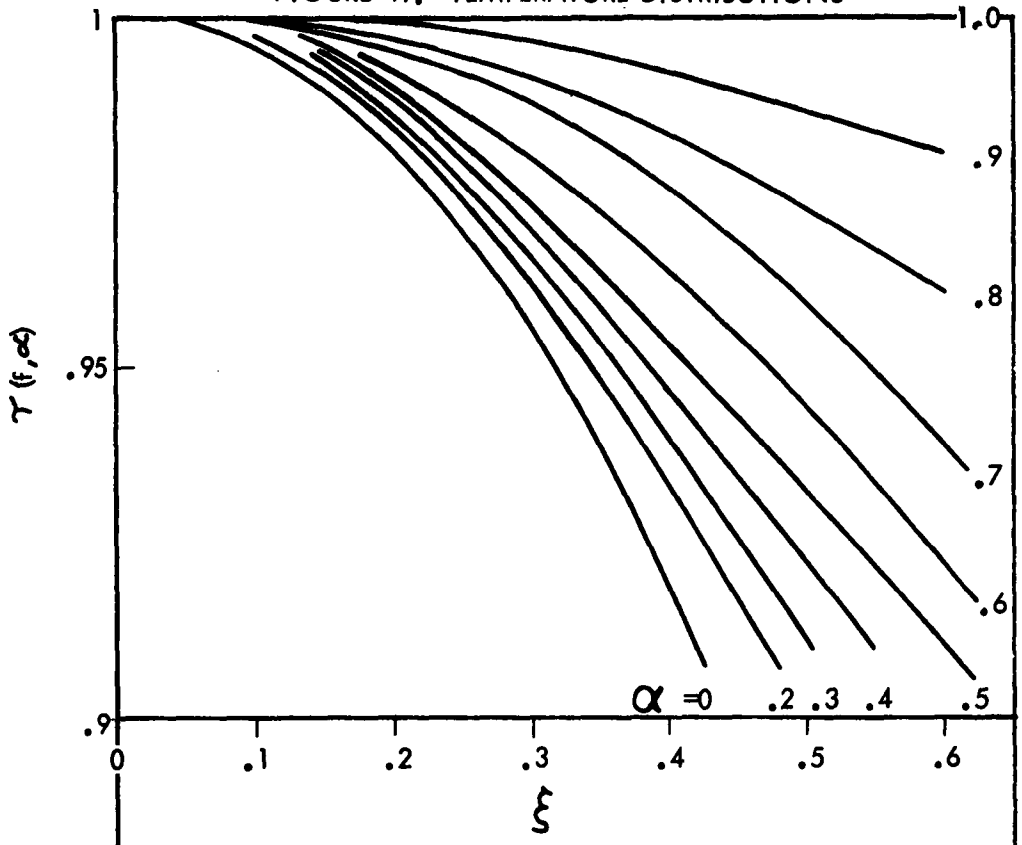

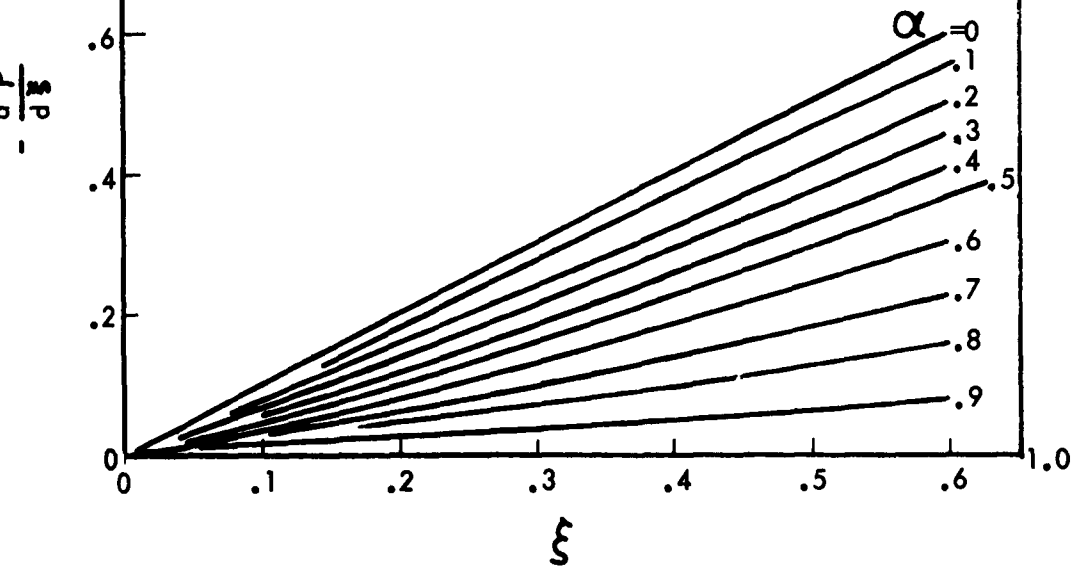

FIGURE 18. DIMENSIONLESS GRADIENTS

120-63-755

To simplify the analysis, the anode was unwrapped as follows:

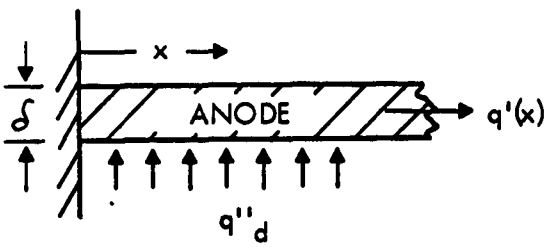

Under the assumptions listed above, the governing differential equation is

$$K\delta \frac{d^2T}{dx^2} - \sigma\epsilon FT^4 + q''_d = 0 \ ,$$

with boundary conditions

$$T(o) = T_o \quad \text{and}$$

$$\left(\frac{dT}{dx}\right)_{x = 0} = 0 \ .$$

Introducing the dimensionless variables

$$\tau = \frac{T}{T_o} \ ,$$

$$\xi = x\sqrt{\frac{q''_d}{K\delta T_o}} \ , \quad \text{and}$$

$$\alpha = \sigma\epsilon FT_o^{\ 4}/q''_d \ ,$$

the governing equations reduce to

$$\frac{d^2\tau}{d\xi^2} - \alpha\tau^4 + 1 = 0 \ ,$$

$$\tau(o) = 1 \ , \quad \text{and}$$

$$\tau'(o) = 0 \ .$$

The parameter α is the ratio of radiation heat flux at T_o to the input heat flux. The governing equation cannot be solved in closed form because of its non-linearity; however, approximations can be found for $\alpha << 1$ and near $\alpha \cong 1$. The results of these approximations agree near $\alpha = 0.5$; hence, the solutions obtained are valid for the entire range of α (i.e., $0 \leq \alpha \leq 1$).

The results of the analyses are given in Figures 17 and 18. Figure 17 shows dimensionless temperature distributions, while Figure 18 indicates dimensionless temperature gradients. An example of the use of these curves is given below. Suppose

$$q''_d = 15 \text{ w/cm}^2 = 47{,}700 \text{ Btu/hr-ft}^2 ,$$

$$T_o = 1400^\circ\text{F} ,$$

$$F = 0.85 ,$$

$$\epsilon = 0.85 ,$$

$$K = 65 \text{ Btu/hr-ft}^\circ\text{F} \text{ (for molybdenum at } 1400^\circ\text{F)} ,$$

$$\delta = 0.031 \text{ in.} = 0.00258 \text{ ft} ,$$

$$L = X_{max} = 0.63 \text{ in.} = 0.052 \text{ ft} ;$$

then

$$\alpha = \frac{(0.1713)(0.85)(0.85)\left(\frac{1860}{100}\right)^4}{47{,}700} = 0.311 , \text{ and}$$

$$\xi = 0.052\sqrt{\frac{47{,}700}{65 \times 1860 \times 0.00258}} = 0.642$$

From Figure 17, $\tau = 0.87 = \frac{T_{end}}{T_o}$; hence ,

$$T_{end} = 1860 \times 0.87 = 1620^{\circ}R ,$$

and the temperature variation is then $240^{\circ}F$.

The results of this sample problem indicate that the circumferential temperature variation in a thin anode can be appreciable. It can, of course, be reduced by increasing the thickness of the anode, thus presenting a larger cross sectional area for heat flow. The most feasible way to accomplish this without unduly increasing the radiator weight is to substitute a low density, high conductivity material for part of the anode. From the standpoint of thermionic conversion, only a thin anode layer is required to provide the proper work function; however, it must be thick enough to withstand the cesium environment. Micrometeorite protection unitized to the anode in a non-bumpered configuration will reduce the circumferential temperature variation. Since beryllium satisfies the previously listed requirements (i.e., low density and high conductivity), an integral micrometeorite armor-fin arrangment will diminish this problem. A schematic representation of this configuration is illustrated below.

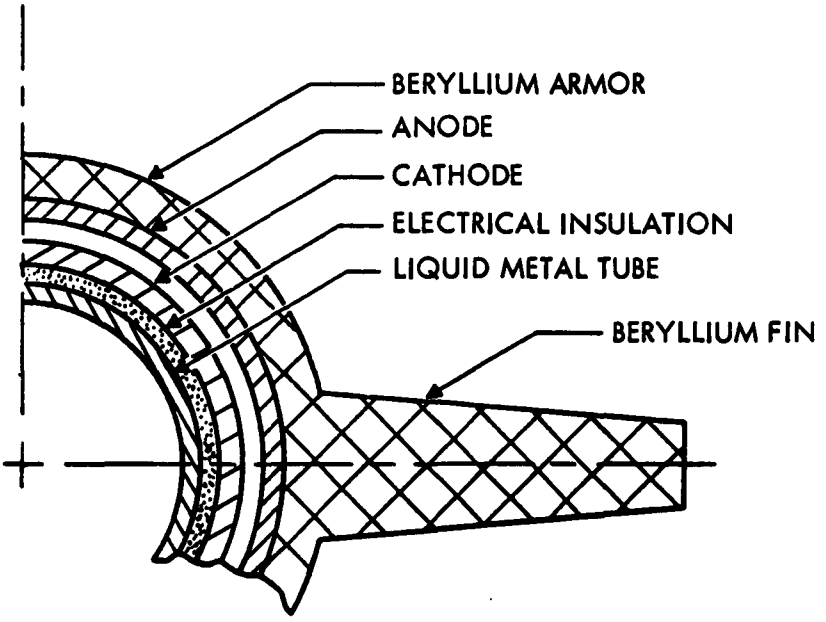

If the thickness of the molybdenum collector is reduced to 0.005 in. and an equivalent weight of beryllium (0.142 in.) is added

$$\xi = 0.052 \sqrt{\frac{47,700}{1860\ (65 \times 0.0004 + 58 \times 0.0118)}}$$

$$= 0.26$$

From Figure 17

$$\tau = 0.975 \text{ ; so}$$

$$T_{end} = 1860 \times 0.975 = 1820^{\circ}R$$

and the temperature variation is only $40^{\circ}F$.

The above example illustrates the need for a continuing analysis of all radiator operating characteristics. Circumferential temperature variation in the collector may present a serious problem. If beryllium is substituted for part of the collector, the severity of the temperature distribution problem may be considerably reduced; however, development of the bond between the molybdenum electrode surface and the beryllium may require as much effort as is currently being applied to the cathode bond problem. Considerations such as these should be continually factored into the development program if generators suitable for use in a radiator system are to be developed.

Nomenclature

q''_d	Incident anode heat flux, $Btu/hr\text{-}ft^2$
q''	Radiation heat flux, $Btu/hr\text{-}ft^2$
σ	Stefan-Boltzmann Constant, 0.1713×10^{-8} $Btu/ft^2\text{-}hr\text{-}^{\circ}F^4$
ϵ	Thermal emissivity of anode surface
F	Radiation view factor
T	Temperature, $^{\circ}F$
X	Distance along anode circumference, ft
δ	Anode thickness, ft
q'	Linear heat transfer rate, Btu/hr-ft
K	Anode thermal conductivity, $Btu/hr\text{-}ft\text{-}^{\circ}F$

2. Reactor Characteristics

The heat source for the thermionic radiator system is a high-temperature, liquid-metal-cooled reactor. Since thermionic generators are very sensitive to emitter temperature, the two reactor characteristics having the greatest effect on the performance of the system are reactor outlet temperature and flow rate through the reactor. Reactor outlet temperature is determined by metallurgical considerations; primarily, the compatibility of the fuel cladding and the fuel itself, and the fuel cladding and coolant. An analysis of these considerations is beyond the scope of the present study. Flow rate through the reactor is a function of reactor geometry and the power available for pumping.

The highest possible flow rate is advantageous from the standpoint of thermionic converter performance, since the higher the flow rate, the less the fluid temperature drop along each radiator tube, and thus all emitters operate nearer the maximum fluid temperature. However, as the flow rate is increased, either the amount of power used to circulate the fluid, or the size of the reactor must be increased, both of which tend to increase over-all system weight. The correlation among reactor size, coolant flow rate, and pumping power input must be known to determine the optimum operating conditions, and the compromise that is necessary among converter performance, pump power (and weight), and reactor weight.

For the purposes of this analysis, the reactor is assumed to be a uranium carbide fueled, fast reactor. The critical size of such a reactor is essentially a function of the fraction of the core occupied by fuel, as the effect of the coolant and structural material is minor. The results of calculations of critical size as a function of reactor fuel fraction are shown in the following table.

TABLE 1

URANIUM-CARBIDE FUELED REACTOR SIZE
(Length to diameter ratio = 1.2)

Fuel Fraction	Core Diameter, cm	Core Length, cm
0.76	21.5	25.8
0.54	22.5	27.0
0.39	24.0	28.8

From geometry considerations, the number of fuel pins in each reactor type is assumed to be 475. The pin diameter can be calculated from the fuel fraction and reactor size, and if the cladding thickness is known, the fraction of the core remaining for coolant passages can be calculated. The following table gives a summary of those parameters for a fuel cladding of 0.016.

TABLE 2

REACTOR PIN SIZE AND COOLANT FRACTION

Fuel Fraction	Fuel Diameter (inches)	Pin OD (inches)	Coolant Fraction
0.76	0.315	0.347	0.20
0.54	0.331	0.363	0.25
0.39	0.355	0.387	0.33

The pump work required to circulate the coolant through the active core can now be calculated as a function of reactor power level and temperature difference through the core (Figure 19). The total reactor pressure drop was estimated as twice the pressure drop in the active reactor fuel bundle.

Core size is plotted as a function of pump work for various power levels coolant temperature difference ratios. To determine the optimum operating point, it is necessary to express pump work and core size in terms

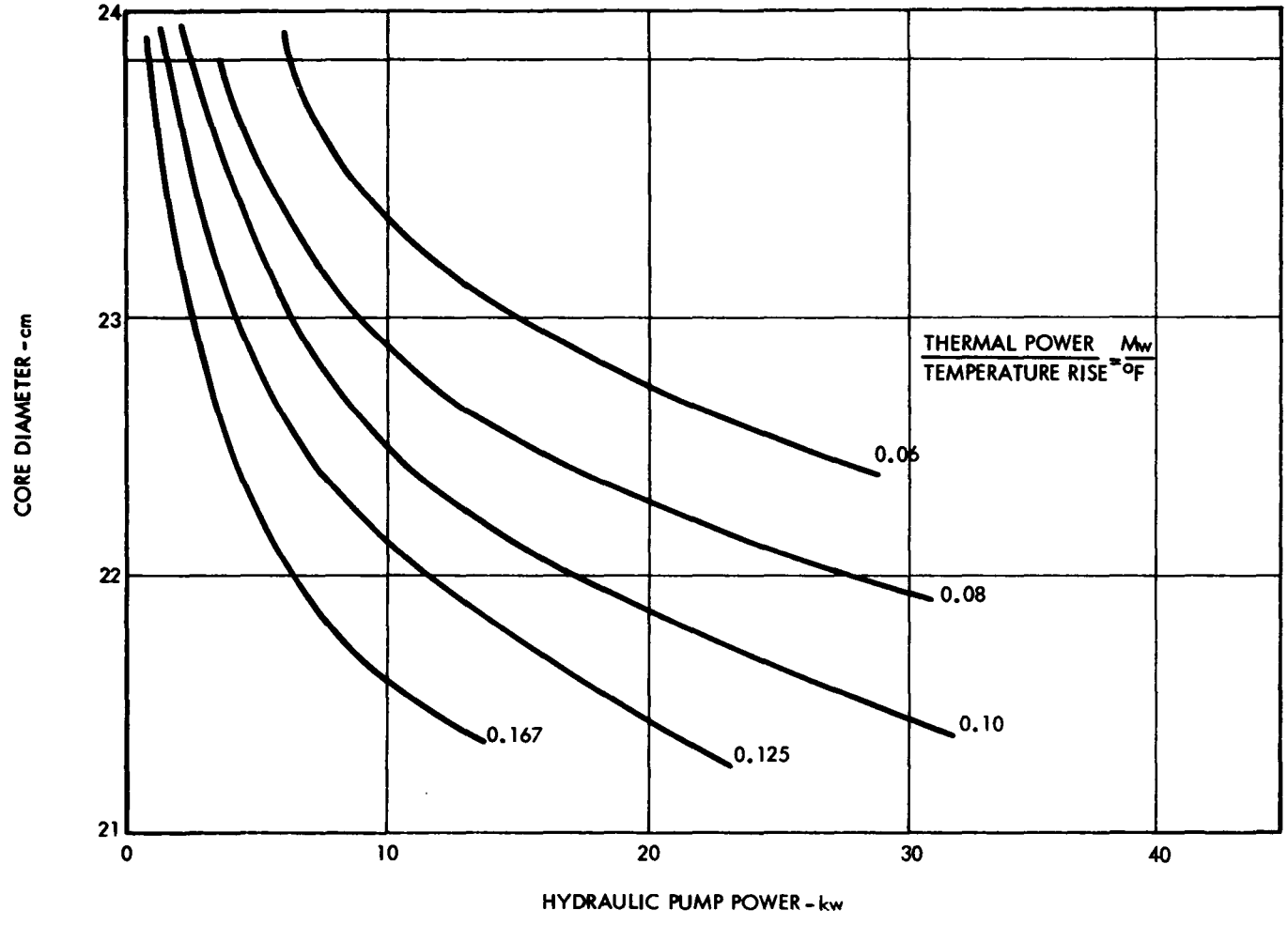

FIGURE 19. REACTOR FLOW CHARACTERISTICS

of component weights, and coolant temperature difference in terms of converter performance and ultimately in terms of radiator weight. Optimum conditions can then be selected on the basis of minimum over-all system weight. This cannot be accomplished until the analysis of degradation of converter power and efficiency during series operation is completed.

C. TASK 4 - SERIES UNIT LOOP TEST

1. General Loop Configuration

A natural-convection loop has been designed with the following characteristics:

Maximum design temperature	2200°F (1204°C)
Minimum (cold leg) temperature	1940°F (1060°C)
Tube OD	0.75 in.
Tube ID	0.62 in.
Over-all height	67 in.
Thermal power input	12.1 kw
Flow rate	120 lb/hr
Flow velocity	0.50 ft/sec
Temperature drop through one converter (assuming 500 watt load)	14.4°F (8°C)
Total temperature drop through converters (no reheat)	43.2°F (24°C)

The general loop configuration is shown in Figure 20. All loop components in contact with the lithium heat transfer fluid are fabricated of columbium-1% zirconium. All heating and cooling is done in the sections that are nearly horizontal. The hot and cold vertical sections operate at essentially maximum and minimum loop temperatures for nearly the full vertical height of the loop. This results in the maximum driving force for a given temperature difference.

The loop is supported on a stainless steel stand that is in turn bolted to the vacuum chamber. The loop is rigidly connected only at one point, the center of the right hand heat sink unit. The left hand heat sink unit is retained in the vertical direction, but is free to move in the horizontal plane. The lower section of the loop is free to move about 1/2 inch in the horizontal plane and is spring loaded in the vertical direction.

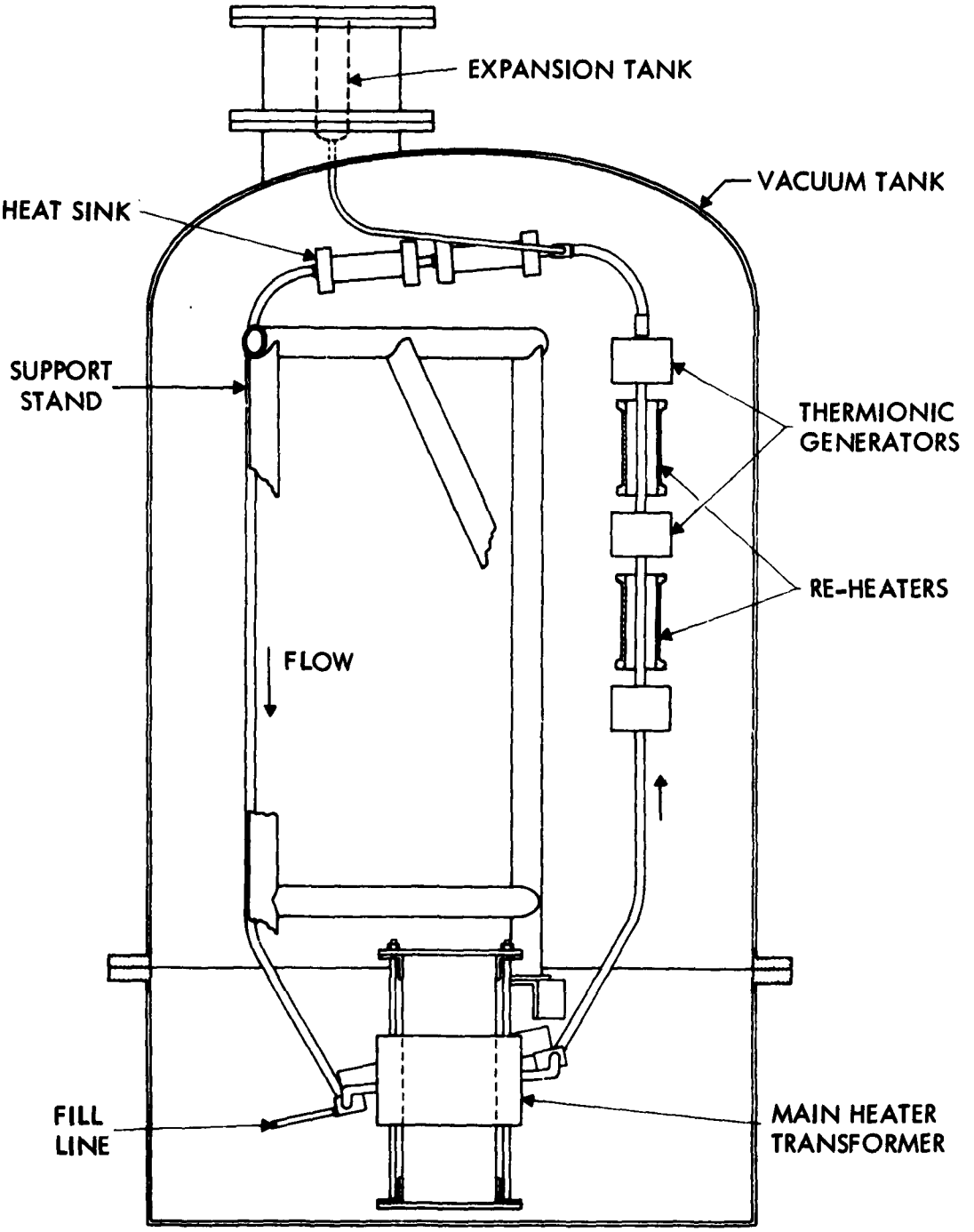

FIGURE 20. SERVICES UNIT TEST LOOP

169-63-07.1

Descriptions of the major loop components follow.

2. Main Heater

Heat is supplied to the loop by electrical resistance heating in the lower section. A high current is induced in this section by a transformer that is located inside the vacuum tank: the loop forms the secondary winding of the transformer. A molybdenum bar completes the electrical current circuit and prevents all but a small amount ($\approx$30 amps) of the induced current from passing up through the thermionic units. The size of the molybdenum bar is adjusted so that the resistance heating in the bar just compensates for thermal conduction from the hot side to the cold side of the loop.

3. Heat Sink

Heat must be removed from the lithium at the top of the loop to establish the temperature difference, which in turn induces circulation in the lithium. Heat is removed by conduction through a concentric tube mounted on the columbium tube (see Figure 21). A large temperature drop is established in the cylindrical section so the heat can be removed from the tips of the cylinder by water cooling at about 100°F. The thickness and length of the cylindrical section has been adjusted so that slightly more than 10 kw will be removed in the entire heat sink.

The cylinders are slotted to eliminate circumferential rigidity and thereby reduce thermal stress. The use of copper instead of molybdenum for a large part of the cylinder also tends to reduce thermal stress.

The joints between columbium, molybdenum, and copper will be brazed to insure good heat transfer. Brazing techniques developed in Task 2 will be used for the columbium-to-molybdenum braze.

4. Surge Tank

A surge tank is provided at the top of the loop to compensate for thermal expansion of the lithium and to provide a means of evacuating and pressurizing the loop. The tank will be made of stainless steel. The transition from columbium to stainless steel will be made using a special Marmon flange fitting in which one flange is stainless steel and

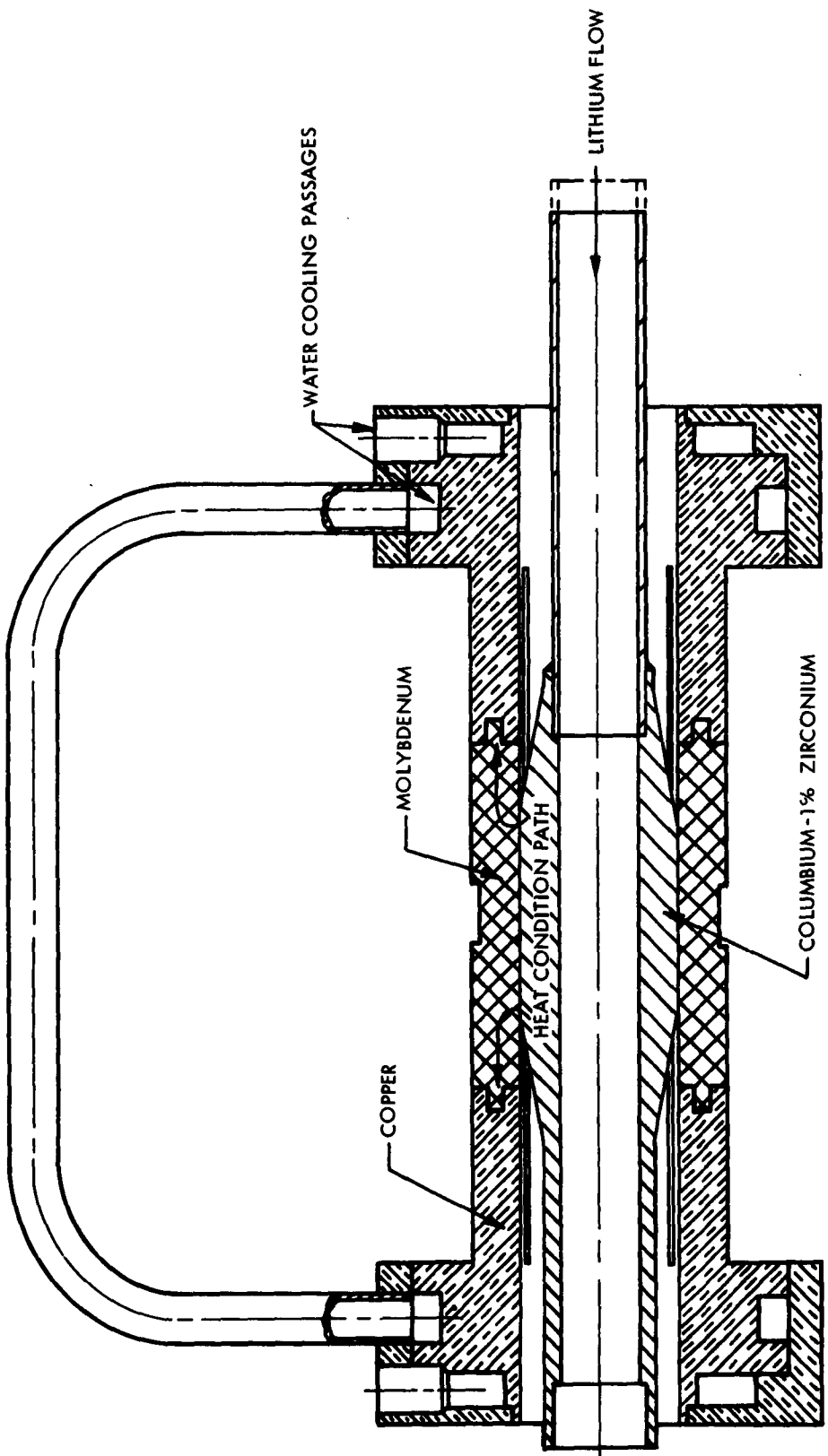

FIGURE 21. HEAT SINK ASSEMBLY

the other is columbium.

A port is provided at the top of the surge tank through which the loop can be evacuated or filled with argon. Level probes are also provided in the surge tank to indicate the proper filling level.

5. Thermionic Generators

Three thermionic generators will be mounted near the top of the hot leg of the loop. The lithium temperature at the inlet of the first converter will be essentially maximum loop temperature. The electrical output of the converters will be led outside the tank using 0.5 in. solid copper conductors. The output will be dissipated in large carbon bar resistors. Provision will be made for both independent and series operation of the converters.

The converters to be used in this loop are identical to those being developed for ASD by RCA under Contract AF 33(657)-8005. These converters are described in RCA's fourth quarterly technical report and will therefore not be described in detail here. However, the general specifications of the converter are given below.

1) The converter emitter will be molybdenum.

2) The center mounting tubing will be columbium-1% zirconium.

3) The entire converter assembly will be capable of withstanding a temperature of 500°C without deleterious effect.

4) The converter will employ a concentric cylindrical configuration as follows:

Emitter OD	0.85 to 1.050 inches
Emitter active length	2.0 to 2.5 inches
Emitter area	40 cm^2
Converter length (not including tubing)	4.25 inches maximum

IV. FUTURE PLANS

The following work is planned for the next quarter.

A. TASK 3 - THERMAL TRANSPORT ANALYSIS

This task will be completed during the next quarter.

B. TASK 4 - SERIES UNIT LOOP TEST

Loop fabrication will be completed during the next quarter. The thermionic converters will be installed in the loop and preparations for loop operation will be started.

DISTRIBUTION LIST

Cys	ACTIVITIES AT WPAFB
1	ASAPT
1	ASAPR
1	ASRMFP
3	ASRMFP-2 (Capt. Redden)
1	ASRNET
	OTHER DEPT OF DEFENSE ACTIVITIES
	Navy
1	Office of Naval Research Code 429 ATTN: Lt. Cmdr. John J. Connelly Washington 25, D. C.
	Air Force
1	AFCRL (CRZAP) ATTN: Mr. A. W. Diniak L. G. Hanscom Field Bedford, Massachussetts
1	AFOSR (SRHPM) ATTN: Dr. Milton Slawsky Bldg. T-D Washington 25, D. C.
1	SSD (SSTRE, Capt. W. Hoover) AF Unit Post Office Los Angeles 45, California
22	ASTIA (TIPDR Arlington Hall Stn Arlington 12, Virginia

Cys	OTHER U.S. GOVT. AGENCIES
1	U.S. Atomic Energy Commission Division of Reactor Development ATTN: Cmdr. W. Schoenfeld Washington 25, D. C.
1	Advanced Research Projects Agency ATTN: Dr. John Huth Washington 25, D. C.
1	Jet Propulsion Laboratory Spacecraft Secondary Power Section ATTN: Mr. Paul Goldsmith 4800 Oak Park Drive Pasadena, California
1	Aerospace Corporation ATTN: Library Technical Document Group Post Office Box 95085 Los Angeles 45, California
1	NASA - Lewis Research Center ATTN: Mr. Roland Breitweiser 210000 Brookpark Road Cleveland 35, Ohio
	OTHERS
1	Hughes Research Laboratories ATTN: Dr. Roland Knechtli Malibu, California
1	Babcock and Wilcox Company ATTN: Mr. P. F. Schutt P. O. Box 1260 Lynchburg, Virginia
1	Radio Corporation of America ATTN: Mr. F. G. Block Electronic Tube Division Lancaster, Pennsylvania